Effect of pycnocline thickness on internal solitary wave breaking over a slope

Nakayama, Keisuke

Iwata, Ryo

Shintani, Tetsuya

(Citation)
Ocean Engineering,230:108884

(Issue Date)
2021-06-15

(Resource Type)
journal article

(Version)
Accepted Manuscript

Effect of pycnocline thickness on internal solitary wave breaking over a slope

Keisuke Nakayama[1], Ryo Iwata[1], and Tetsuya Shintani[2]

[1] *Kobe University, 1-1 Rokkodai-Cho, Nada-Ku, Kobe-Shi, Kobe 657-0013, Japan*

[2] *Tokyo Metropolitan University, 1-1, Minami-Osawa, Hachioji-Shi, Tokyo 192-0397, Japan*

Abstract

When an internal solitary wave (ISW) breaks over a sloping bottom in the ocean, turbulent mixing causes energy dissipation that is associated with the breaking type. In a two-layer fluid, when pycnocline thickness is negligible, the breaking can be categorized into one of four breaker types: surging, plunging, collapsing, and fission breakers. The latest classification into four breaker types is based on wave slope, bottom slope gradient and an internal Reynolds number. However, it was unknown if this classification can be applied to categorize the breaking of an ISW under thick pycnocline conditions. The present study uses two-dimensional numerical simulations to investigate energy dissipation due to an ISW breaking over a slope under changing pycnocline thickness. We found that the classification can categorize all breaker types even when pycnocline thickness varies. Also, the practical reflection coefficient, defined in this study, becomes smaller for collapsing and surging breakers with the increase in the pycnocline thickness due to an offshore shift in breaking points. In contrast, the practical reflection coefficient is found to be constant for plunging and fission breakers under changing pycnocline thickness.

Keywords: *internal wave; classification; reflection coefficient; energy dissipation; numerical simulation*

1. INTRODUCTION

Internal waves play a significant role in resuspension and transport of particulate matter due to breaking over sloping bottoms in lakes and the ocean (Boegman and Stastna, 2019). Resuspension of particulate matter due to internal waves has been demonstrated with high-resolution field observations in Lake Erken (Pierson and Weyhenmeyer, 1994). The study found that epilimnion mixing induces resuspension due to internal seiches in the benthic boundary layer. These internal seiches have also been shown to cause high-frequency internal waves, which drive resuspension over the bottom of Lake Alpnach (Gloor et al., 1994). Pineda (1994) demonstrated that mass transport in both offshore and onshore directions occurs due to the breaking of high-frequency internal waves over a topographical slope based on the observed vertical profile of density and horizontal velocity in southern California. Davis and Monismith (2011) also showed that the several different breaking types of internal waves potentially exhibit a broad range of turbulence strength and energy dissipation, which affected the resuspension of particulate matter in the outer southeast Florida shelf. In particular, internal solitary waves (ISWs) have been shown to significantly influence energy dissipation over sloping bottoms (Helfrich and Melville, 2006; Lamb, 2014). Therefore, it is useful to investigate the characteristics of ISW breaking over a sloping bottom, such as energy dissipation, in lakes and the ocean.

Many laboratory experiments have been conducted related to the breaking of ISWs over slopes. Horn et al. (2001) investigated the deformation of low-frequency internal waves into a train of ISWs using a tilting tank, in which the upper layer thickness was thinner than the lower layer. Using the same tilting tank as Horn et al. (2001), Boegman et al. (2005) showed that breaking over a sloping bottom leads to localized turbulent mixing and enhanced energy dissipation, which transfers energy from a basin-scale seiche to ISWs and small scale dissipation. Regarding the interaction between internal waves and a sloping bottom boundary, Michallet and Ivey (1999) found that the reflection of incident energy from an ISW over a slope, which is associated with energy dissipation, is a function of the wavelength of the ISW and slope length. By carrying out additional laboratory experiments and numerical simulations similar to Michallet and Ivey (1999), Bourgault and Kelly (2007) also revealed that the reflection coefficient of an ISW from a slope is a function of the Iribarren number. Michallet and Ivey (1999) and Bourgault and Kelly (2007) clarified the factors essential for estimating energy dissipation due to ISW breaking over a slope: the ratio of the wavelength of the ISW to slope length and the Iribarren number. However, Bourgault and Kelly (2007) suggested that further studies were necessary to validate the parameter to estimate energy dissipation.

In a previous study related to ISW breaking and energy dissipation over a slope using numerical simulations, Forgia et al. (2018) found that the reflection coefficient varies with the change in breaking type over a sloping bottom, which means that energy dissipation may be associated with breaking types. Additionally, Forgia et al. (2020) revealed that the reflection coefficient decreases with the increase in the pycnocline thickness using numerical simulations. Aghsaee et al. (2012) demonstrated that vortex shedding beneath ISWs over the bottom depends on a non-dimensional pressure gradient and the momentum-thickness Reynolds number at the separation point, which may change the breaking type of an ISW over a slope. Nakayama et al. (2012) investigated mass transport due to the breaking of an ISW over a slope, which revealed that the larger the quadratic nonlinear coefficient of the KdV equation the more extensive the energy dissipation becomes. They also showed that energy dissipation increases with a decrease in the slope gradient using a critical amplitude (Nakayama and Imberger, 2010), which may suggest that the breaking type of an ISW is related to energy dissipation. Therefore, the prediction of the breaking type of an ISW over a sloping bottom is crucial for estimation of energy dissipation.

In terms of the breaking type of ISWs over a slope, Boegman et al. (2005) proposed three types of breaking by setting up a slope in the tilting tank used by Horn et al. (2001): spilling, plunging and collapsing breakers. They also proposed an internal Iribarren number to classify the breaking type of an ISW over a slope by modifying the Iribarren number by Galvin (1968). On the other hand, Aghsaee et al. (2010) proposed a new categorization of breaker types for ISW over slopes using numerical simulations. They demonstrated that four breaker types (surging, plunging, collapsing and fission breakers) could be classified based on bottom slope gradient and wave slope. Sutherland et al. (2013) found difficulty in categorizing their results according to bottom slope gradient and wave slope only. They suggested the application of the internal Iribarren number to classify all breaker types. However, Nakayama et al. (2019) showed that the classifications by Aghsaee et al. (2010) and Sutherland et al. (2013) could not categorize breaking in the laboratory experiments by Boegman et al. (2005).

Aghsaee et al. (2012) revealed that viscosity at the bottom boundary controls whether or not collapsing or plunging breakers occur. Furthermore, Shroyer et al. (2009), Saffarinia and Kao (1996) and Nakayama et al. (2012) suggested the importance of critical depth on residual currents and breaking of an ISW in numerical simulations (Tsuji and Oikawa, 2007). Critical depth is the depth where a conjugate flow appears, which was shown by Lamb and Wan (1998). Tsuji and Oikawa (2007) also showed the importance of critical depth on the excitation and deformation of an ISW. The critical depth is located in the middle of the total water column in a two-layer fluid under the Boussinesq approximation. Shroyer et al. (2009) explored ISWs from shipboard measurements off the coast of New Jersey and found deformation of depression waves into elevation waves at a critical point (critical depth). Based on these findings, Nakayama et al. (2019) proposed a new parameter, an internal Reynolds number, by combining the quadratic term coefficient of the KdV equation and the traditional Reynolds number based on wave speed, which indicates the effects of critical depth and viscosity. The internal Reynolds number was found to classify all breaker types by combining with bottom slope gradient and wave slope. However, application only to two-layer fluids with a thin pycnocline condition has been discussed so far, and applicability of the classification to the ocean remains unresolved. The effect of breaking type on energy dissipation also needs to be clarified by exploring changing pycnocline thicknesses.

This study thus aims to investigate whether Nakayama's classification can categorize breaker types when pycnocline thickness varies, and to clarify the effect of pycnocline thickness on an ISW breaking over a slope. First, we adjusted four physical parameters, density ratio, bottom slope gradient, wave slope and the internal Reynolds number to simulate four breaker types' conditions using Nakayama's classification with the thin pycnocline thickness. Then, we investigated four breaker types over a slope by changing pycnocline thickness to clarify the thickness's influence on breaker types. Second, breaking points where the vertical pressure gradient becomes zero were verified by comparing with the general breaking location defined in previous studies (Lamb, 2014; Boegman et al., 2005) when pycnocline thickness varies. Finally, the effect of pycnocline thickness on reflection of an ISW from a slope was investigated under changing pycnocline thickness to evaluate energy dissipation due to the breaking of an ISW over a slope. Note that we used two different parameters regarding reflection from a slope, "practical reflection coefficient" and "reflection coefficient". The practical reflection coefficient is defined in this study to understand the peak energy ratio of reflected and incident internal waves, with the reflection coefficient defined as by Michallet and Ivey (1999), for example, as the spatially-integrated energy ratio of a reflected and incident internal waves.

2. METHODS

2.1. Numerical simulations

A three-dimensional non-hydrostatic model, Fantom, was used to analyze the breaking of shoaling internal solitary waves (Nakayama et al., 2014; Nakayama et al., 2016; Nakayama et al., 2019). Fantom is an object-oriented parallel simulator for the analysis of environmental fluid flows, employing a turbulence closure scheme option, a $k-\varepsilon$ turbulence closure scheme (Jones and Launder, 1972; Umlauf and Burchard, 2003). A free surface was applied to the top boundary, and a no-slip condition was given on the bottom and sloping boundaries, respectively. The partial cell scheme was used to represent a uniform bottom slope in the z-coordinate model (Adcroft et al., 1997). According to previous studies (Nakayama and Imberger, 2010; Arthur and Fringer, 2014), the local turbulent dissipation in the breaking zone is about 3×10^{-6} to 10^{-5} m^2 s^{-3} for a laboratory scale, which gives a corresponding Kolmogorov length scale of 0.56 to 0.76 mm. In the breaking zone, we used 2 mm grid sizes in a vertical cross-section, which is a factor of about three compared to the Kolmogorov length scale. Additionally, since the $k-\varepsilon$ turbulence closure scheme has problems in reproducing flows in low-Reynolds number regions, including bottom boundary layers, we decided to apply direct numerical simulations. The use of two-dimensional numerical simulations does not capture three-dimensional processes such as secondary instability, and a three-dimensional computation is important for the accurate estimation of energetics due to breaking (Arthur and Fringer, 2014). Arthur and Fringer (2014) showed that a three-dimensional simulation had about 8 % more energy dissipation compared to a two-dimensional simulation. In previous studies, two-dimensional simulations were validated through investigation of shoaling mode 1 waves onto a shelf, such as overturning and shear instabilities over a slope (Vlasenko and Hutter, 2002; Bourgault and Kelley, 2007; Aghsaee et al., 2012; Lamb, 2014). We attempt to investigate the breaking criteria by comparing it with that obtained using two-dimensional numerical simulations by Aghsaee et al. (2010). Also, we aimed to validate energy dissipation by comparing with Bourgault and Kelly (2007), in which a two-dimensional simulation was applied. Therefore, the two-dimensional vertical computational domain was used to investigate the breaking of an ISW over a slope in the same manner as in Nakayama et al. (2019). It should be noted that the available potential and kinetic energy analysis in this study may show an underestimation of energy dissipation by up to a maximum of about 8 %.

We applied the hyperbolic-tangent function into a vertical profile of density to give different pycnocline thickness (Eq. (1)).

$$\rho(z) = \rho_1 + 0.5\Delta\rho\left[1 + \tanh\left(\frac{z - h_2}{a_I/2}\right)\right], \tag{1}$$

where ρ is the density, z is the upward-positive vertical coordinate with an origin at the flat bottom, h_1 and h_2 are the upper and lower layer thicknesses, ρ_1 and ρ_2 are the densities of the upper and lower layers, $\Delta\rho = \rho_2 - \rho_1$, and a_I is the thickness of the pycnocline.

To generate a stable ISW, we gave a flat bottom length of 3 m for all cases. The horizontal and vertical grid sizes over the slope were 0.002 m x 0.002 m, and the maximum grid size was 0.02 m x 0.01 m adjacent to the flat bottom close to the wave generator to save computational time (Fig. 1). The spanwise single grid size was set at 0.02 m ($= B_e$). We applied Mirie and Pennell (1989) to generate an ISW based on third-order solutions (Appendix in Nakayama et al. (2019)), which gives sufficient accuracy similar to the Dubreil-Jacotin-Long equation (Aghsaee et al., 2010; Nakayama et al., 2019). Fluxes to generate an ISW were given in the upper and lower layers with thicknesses of 0.04 m and 0.12 m, respectively (Fig. 1 and Eq. (2)).

$$Q_1 = -Q_2 = -C_R\frac{\partial\eta}{\partial t}\Delta t B_e, \tag{2}$$

where Q_1 and Q_2 are the fluxes in the upper and lower layers, C_R is the wave speed of an internal solitary wave, η is the density interface displacement given by Mirie and Pennell (1989), and Δt is the time step in a numerical simulation.

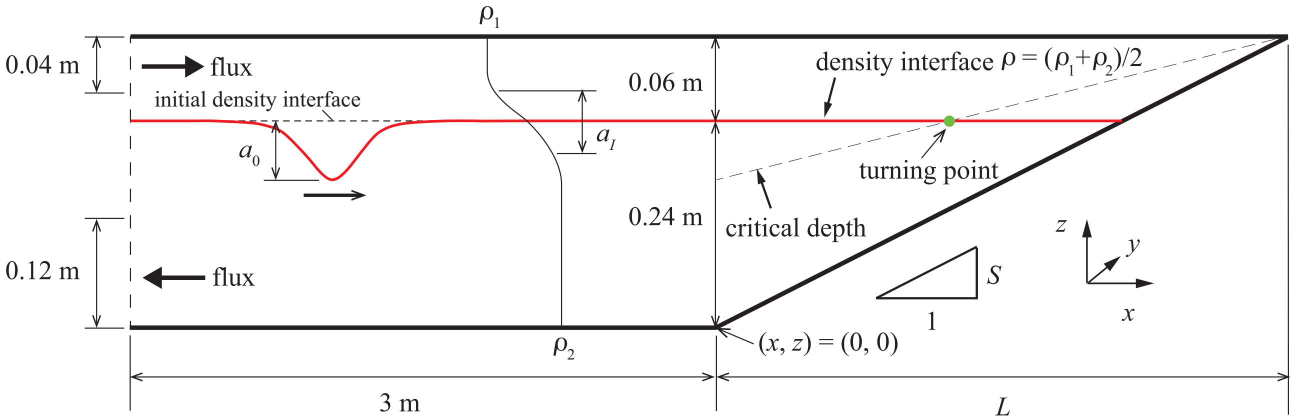

Fig. 1. Computational domain to analyze breaking of an internal solitary wave.

2.2. Analytical methods

Cases S-#, C-#, P-# and F-# correspond to surging, collapsing, plunging and fission breakers, respectively (Table 1). Note this case categorization is based on the classification confirmed with thin pycnocline condition (Nakayama et al. (2019) and we will discuss the effect of pycnocline thickness on the breaking classification. Also, cases AS-#, AC-#, AP-# and AF-# correspond to surging, collapsing, plunging and fission breakers. For cases S-#, C-#, P-# and F-#, the numbers # = 1 to 8 indicate eight different pycnocline thicknesses, a_I, of 0.01 m, 0.02 m, 0.03 m, 0.04 m, 0.06 m, 0.08 m, 0.10 m and 0.12 m, respectively (Table 1 and Table 2). Cases S-#, C-#, P-# and F-# (# = 1 to 8) were selected to investigate the effect of pycnocline thickness on ISW breaking over a slope in detail. For cases AS-#, AC-#, AP-# and AF-#, two pycnocline thicknesses were given in # = 1 and 2, a_I, of 0.01 m and 0.12 m, to understand the difference between two extreme cases: thin and thick pycnoclines. When $a_I = 0.12$ m, the thickest pycnocline condition, the pycnocline reached the water surface. Classification indices were bottom slope gradient S, wave slope $\mathrm{S}_w = a_0/\lambda$ and an internal Reynolds number $\mathrm{Re}_{\mathrm{ISW}} = \alpha_1 h'/\nu$ (Nakayama et al., 2019) (Fig. 2). Here, a_0 is the amplitude of an ISW over a flat bottom just before where the bottom slope starts, ν is the viscosity, λ is the incident-wave wavelength (Koop and Butler, 1981) defined as

$$\lambda = \frac{\int_{-\infty}^{+\infty} \eta dx}{a_0}, \tag{3}$$

α_1 is the coefficient of the nonlinear term in the KdV equation defined as

$$\alpha_1 = \frac{3}{2}\frac{c_0}{h_1 h_2}\frac{\rho_1 h_2^2 - \rho_2 h_1^2}{\rho_1 h_2 + \rho_2 h_1}, \tag{4}$$

c_0 is the linear longwave speed, and h' is the representative depth in a two-layer fluid defined as

$$h' = \frac{h_1 h_2}{h_1 + h_2}. \tag{5}$$

In numerical simulations, densities of the upper layer, ρ_1, were 1000 kg m^{-3}.

Table 1. Computational conditions.

	ρ_2 (kg m^{-3})	h_1 (m)	h_2 (m)	L (m)	ε	S
case S	1020	0.06	0.24	1.0	0.02	0.30
case C	1010	0.06	0.24	2.5	0.01	0.12
case P	1020	0.06	0.24	2.5	0.02	0.12
case F	1020	0.06	0.24	6.0	0.02	0.05
case AS	1010	0.08	0.22	1.5	0.01	0.2
case AC	1010	0.06	0.24	3.0	0.01	0.1
case AP	1010	0.08	0.22	3.0	0.01	0.1
case AF	1020	0.08	0.22	10.0	0.02	0.03

Table 2. Breaking types and computational conditions.

Φ_{P_I} and Φ_{P_R} indicate incident and reflected energy, and S_w indicates wave slope.

	a_I (m)	a_0 (m)	λ (m)	S_w	ξ_I	Φ_{T_R}/Φ_{T_I}	breaking type
case S-1	0.01	0.0184	0.714	0.0257	1.87	0.858	surging
case S-2	0.02	0.0189	0.682	0.0278	1.80	0.830	
case S-3	0.03	0.0194	0.706	0.0275	1.81	0.809	
case S-4	0.04	0.0197	0.703	0.0281	1.79	0.796	
case S-5	0.06	0.0200	0.715	0.0280	1.79	0.781	
case S-6	0.08	0.0199	0.737	0.0270	1.83	0.773	
case S-7	0.10	0.0195	0.775	0.0252	1.89	0.769	
case S-8	0.12	0.0190	0.785	0.0242	1.93	0.752	
case C-1	0.01	0.0148	0.746	0.0199	0.85	0.574	collapsing
case C-2	0.02	0.0153	0.751	0.0204	0.84	0.546	
case C-3	0.03	0.0157	0.747	0.0210	0.83	0.532	
case C-4	0.04	0.0160	0.740	0.0216	0.82	0.502	
case C-5	0.06	0.0162	0.765	0.0212	0.82	0.488	
case C-6	0.08	0.0160	0.788	0.0203	0.84	0.471	
case C-7	0.10	0.0157	0.806	0.0194	0.86	0.458	
case C-8	0.12	0.0152	0.858	0.0177	0.90	0.440	
case P-1	0.01	0.0395	0.623	0.0634	0.48	0.422	plunging
case P-2	0.02	0.0405	0.618	0.0655	0.47	0.411	

case P-3	0.03	0.0414	0.608	0.0681	0.46	0.400	
case P-4	0.04	0.0422	0.593	0.0711	0.45	0.409	
case P-5	0.06	0.0433	0.620	0.0698	0.45	0.396	
case P-6	0.08	0.0438	0.617	0.0710	0.45	0.392	
case P-7	0.10	0.0438	0.638	0.0686	0.46	0.365	
case P-8	0.12	0.0434	0.660	0.0658	0.47	0.371	
case F-1	0.01	0.0161	0.719	0.0223	0.33	0.299	
case F-2	0.02	0.0166	0.722	0.0230	0.33	0.259	
case F-3	0.03	0.0170	0.739	0.0230	0.33	0.251	
case F-4	0.04	0.0173	0.731	0.0236	0.33	0.246	fission
case F-5	0.06	0.0175	0.776	0.0226	0.33	0.245	
case F-6	0.08	0.0173	0.791	0.0219	0.34	0.253	
case F-7	0.10	0.0170	0.785	0.0216	0.34	0.253	
case F-8	0.12	0.0170	0.785	0.0216	0.34	0.253	
case AS-1	0.01	0.0193	0.988	0.0195	1.43	0.818	surging
case AS-2	0.12	0.0224	1.017	0.0220	1.35	0.656	
case AC-1	0.01	0.0126	0.801	0.0157	0.80	0.544	collapsing
case AC-2	0.12	0.0128	0.898	0.0143	0.84	0.404	
case AP-1	0.01	0.0440	0.858	0.0513	0.44	0.393	plunging
case AP-2	0.12	0.0529	0.817	0.0647	0.39	0.363	
case AF-1	0.01	0.0295	0.901	0.0327	0.17	0.175	fission
case AF-2	0.12	0.0344	0.872	0.0395	0.15	0.157	

As one of our aims was to clarify the influence of the pycnocline thickness on the classification of breaker type, we investigated the location of the breaking point of the ISWs over the slope (Nakayama et al., 2012; Nakayama et al., 2019). We computed the breaking point where the vertical pressure gradient becomes zero inside of the pycnocline. Furthermore, we investigated the variation of energy due to the breaking of ISWs over the slope with changes in pycnocline thickness to clarify the reflection of ISWs from the slope. The energy of a non-breaking ISW consists of available potential energy E_P and kinetic energy E_K (Taileux, 2013).

$$E_P = \int_{\rho_1}^{\rho_2} \frac{g}{2\rho_2} \left[z_\rho(\rho) - z_{\rho_I}(\rho) \right]^2 d\rho, \tag{6}$$

$$E_K = \int_{b_t}^{h_1+h_2} \frac{1}{2} (u^2 + w^2) dz, \tag{7}$$

where g is the gravity acceleration, ρ is the density, z_ρ is the height of the density ρ from the flat bottom, z_{ρ_I} is z_ρ at the initial condition, b_t is the height at the bottom topography, and u and w are the velocities in the x and z coordinates, respectively.

E_K is available in the entire computational domain, but E_P is not available in the breaking zone over a slope because the vertical profile of density becomes unstable over a slope; a typical example is a plunging breaker. Potential energy is available only when densities in the vertical profile at initial condition correspond one-to-one with densities after internal wave motions. We thus compute E_K in the entire region, but E_P in a non-breaking zone only. Therefore, we can estimate the reflection of an incident ISW and the reflected internal waves in the non-breaking zone by using total energy ($E_T = E_K + E_P$) under changing pycnocline thicknesses. On the other hand, since we can compute E_K over the slope, there is the possibility to evaluate the influence of pycnocline thickness on energy transfer from available potential to kinetic energy due to breaking for each breaker type.

3. RESULTS

3.1. Classification of breaker types

Cases #-1 (# is S, C, P and F; $a_I = 0.01$ m) are the typical cases inducing four different breakers: surging, collapsing, plunging and fission breakers, respectively, according to the classification by Nakayama et al. (2019) (Fig. 2 and Fig. 3). Each snap shot was chosen to show its typical breaker type (Fig. 3). In a surging breaker, mixing occurred at the front of the wave, and the front ran up the slope accompanying strong mixing. A collapsing breaker is one of the most common breakers in laboratory experiments when the upper-layer thickness is the same as the lower layer in the offshore flat bottom (Nakayama and Imberger, 2010). In the collapsing breaker, the front behaved like a gravity current down slope. Plunging breakers had an apparent rolling over the slope, in which the direction of rotation was opposite to the collapsing breaker. In a fission breaker, several high-frequency internal waves were generated and broke over the slope. In this study, we did not explore a combined type of breakers, such as collapsing-surging and collapsing-plunging breakers (Aghsaee et al., 2010).

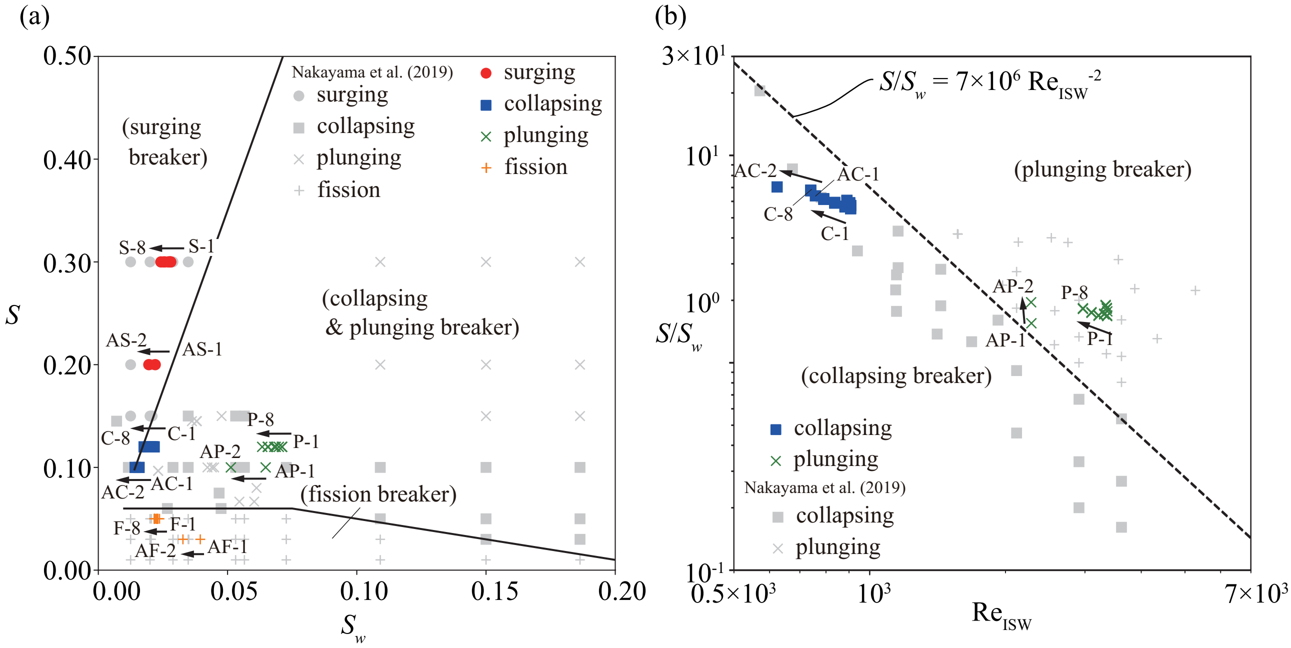

Fig. 2 . (a) ISW breaker types as a function of wave slope S_w and slope gradient S. (b) ISW breaker types as a function of S/S_w and $\mathrm{Re}_{\mathrm{ISW}}$.

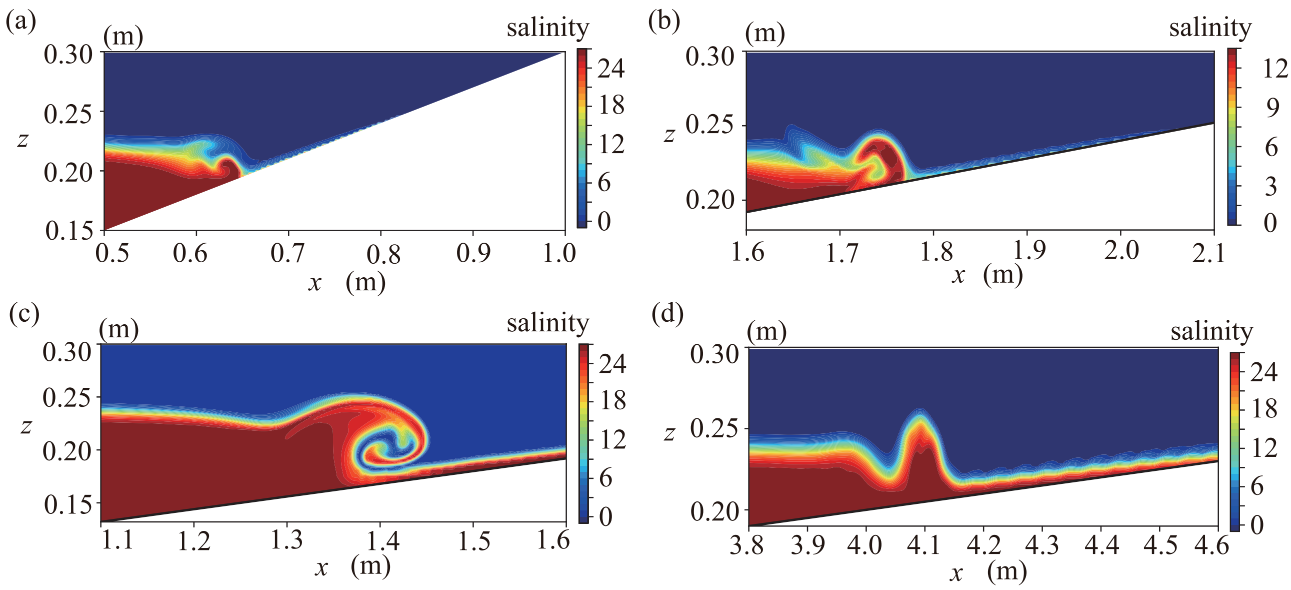

Fig. 3. Breaker types with a pycnocline thickness of 0.01 m. (a) Case S-1: Surging breaker. (b) Case C-1: Collapsing breaker. (c) Case P-1: Plunging breaker. (d) Case F-1: Fission breaker.

There are two useful conceptual parameters, turning point and critical depth to investigate the breaking point of ISWs. Under the Boussinesq approximation, a turning point exists where an initial density interface crosses the critical depth (Fig. 1). The critical depth corresponds to the level where the quadratic term of the KdV equation becomes zero, and the ratio of the layers is $\sqrt{\rho_1}/\sqrt{\rho_2}$. Critical depth is also found in a three-layer fluid from the extended KdV or Gardner equation when the quadratic term is zero and breathers exist (Nakayama and Lamb, 2020). As has been shown in previous studies, breaking points for cases #-1 (# is S, C, P and F; $a_I = 0.01$ m) appeared below the critical depth (Fig. 4). Note that the horizontal and vertical coordinates are normalized with slope length and total depth, respectively in Fig. 4 to plot all breaking points. As found in Nakayama et al. (2019), the breaking points of collapsing and fission breakers appeared onshore from the turning point. On the one hand, the surging breaking point occurred close to the turning point, and the plunging breaking point occurred offshore from the turning point.

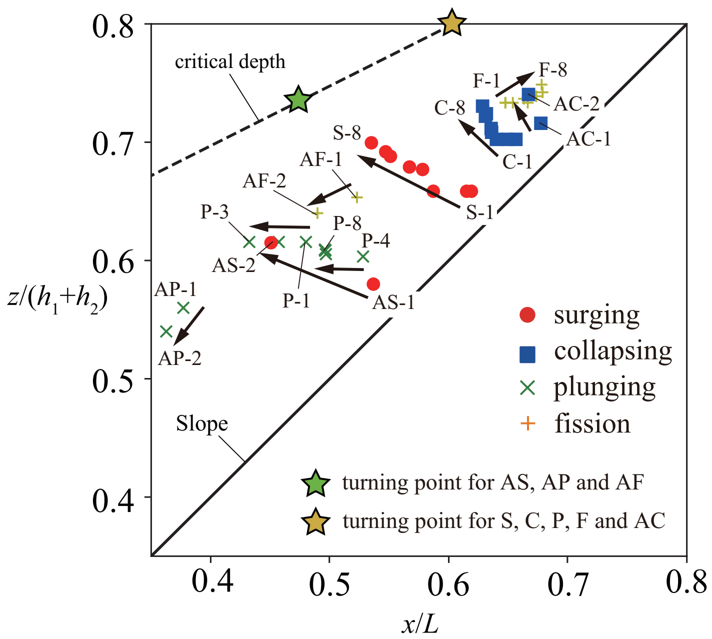

Fig. 4. Breaking points for cases 1-1 to 8-2. Broken line indicates critical depth. Green circles indicate turning points.

To analyze the effect of pycnocline thicknesses on the breaking type, we prepared 8 different thicknesses (from #-1 to #-8) for each breaker type while keeping the wave amplitude almost the same in each type (Table 2). The thicker the pycnocline, the less the specific vertically-integrated density between the upper and lower layers. Namely, the longer the wavelength λ and the smaller the wave slope S_w (Fig. 2). In the classification diagram, although the case C-8 ($a_I = 0.12$ m) appeared close to the classification border between surging, collapsing and plunging breakers, the classification factors for cases S-#, C-#, P-# and F-# (# = 1 to 8) were still confirmed to be valid even with the largest increase in the pycnocline thickness. To see the effect of the pycnocline thickness on the breaking behavior, the breaker types for the cases with a_I = 0.04 m and 0.12 m are shown in Figs. 5 and 6, respectively. In a_I = 0.04 m, there was no change in the surging breaker (Fig. 5a). Collapsing breakers changed to behave like a collapsing-surging breaker, but we could still find the characteristics of a collapsing breaker (Fig. 5b). Plunging breakers had weaker rolling in a_I = 0.04 m compared to a_I = 0.01 m (Fig. 5c). In the fission breaker in a_I = 0.04 m, an ISW generated high-frequency internal waves, which deformed into bolus-type waves that were similar to a_I = 0.01 m (Fig. 5d). In a_I = 0.12 m, breakings occurred in a more extensive region compared to a_I = 0.01 m (Fig. 6). But we found the same characteristics for cases with a_I = 0.12 m as a_I = 0.04 m, and there was no change in all breaker types from a_I = 0.01 m to 0.12 m (Figs. 3, 5 and 6).

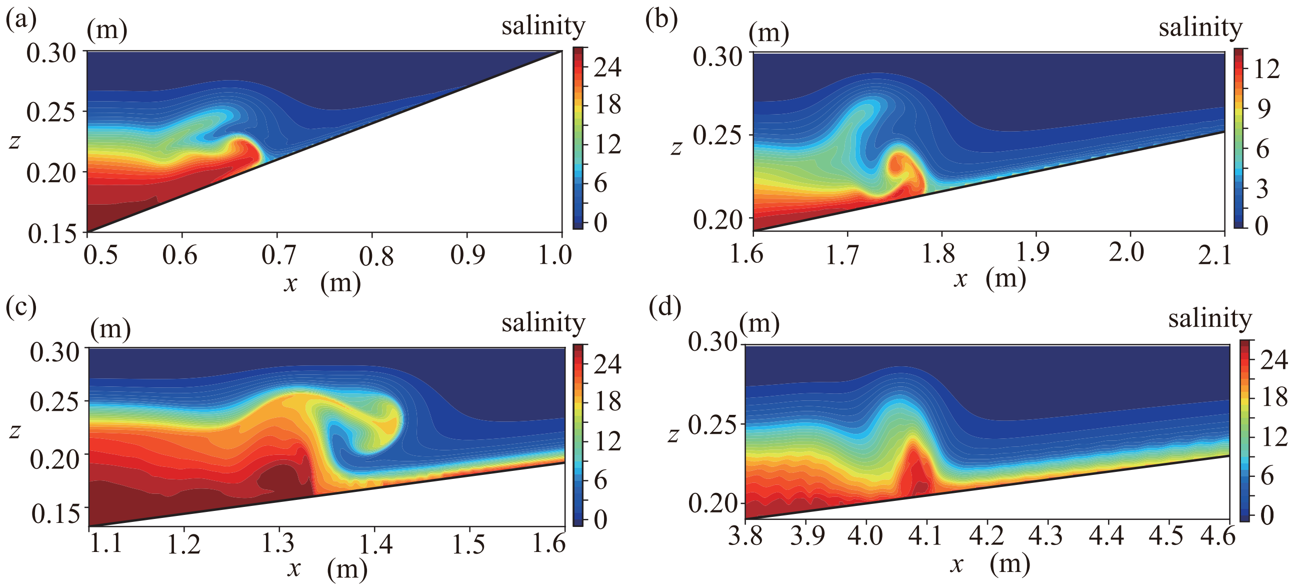

Fig. 5. Breaker types with a pycnocline thickness of 0.04 m. (a) Case S-2: Surging breaker. (b) Case C-2: Collapsing breaker. (c) Case P-2: Plunging breaker. (d) Case F-2: Fission breaker.

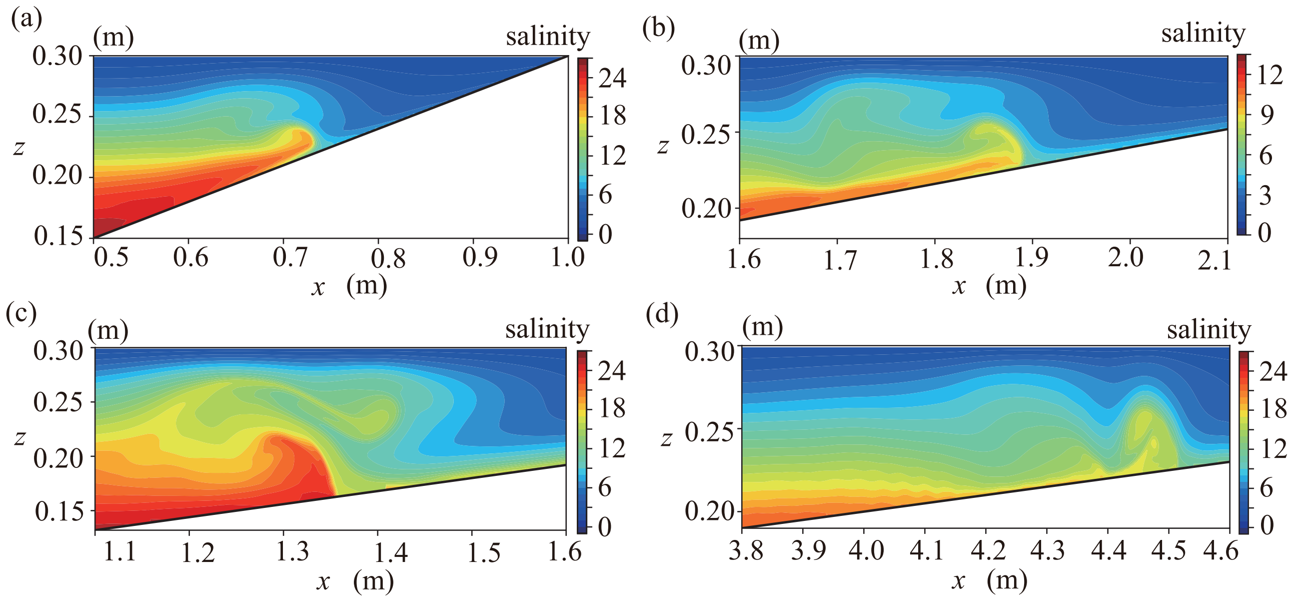

Fig. 6. Breaker types with a pycnocline thickness of 0.12 m. (a) Case S-6: Surging breaker. (b) Case C-6: Collapsing breaker. (c) Case P-6: Plunging breaker. (d) Case F-6: Fission breaker.

For the effect of pycnocline thickness on the breaking point for surging, collapsing and plunging breakers shifted offshore as the pycnocline got thicker for cases S-#, C-# and P-# (# = 1 to 8) (Fig. 4). The breaking points of these breakers were found to appear when an ISW collided with a downdraft in these cases, and the gradient of the density interface at the rear of the ISW became vertical. Since the Brunt–Väisälä frequency decreases with the increase in pycnocline thickness and overturning tends to occur more quickly, the ISWs broke further offshore in the three breaker cases. On the other hand, the breaking point of fission breakers shifted onshore in case F-# (# = 1 to 8) with the increase in the pycnocline thickness. In case F-# (fission breaker), the drawback became thinner and gave less energy to breaking with the increase in pycnocline thickness, which might enhance the onshore shift in the breaking point.

In this study, the breaking point of an ISW was defined as the point where the vertical pressure gradient became zero inside of the pycnocline, which corresponds to a zero-gravity location. In previous studies (Lamb, 2014; Boegman et al., 2005; Dean and Dalrymple, 1991; Helfrich, 1992), the general breaking location (GBL) was defined as being where the rear part of the internal wave becomes vertical for surging, collapsing and plunging breakers and where the first wave of elevation emerges for fission breaker (Aghsaee et al., 2010) (note that 0.28 and 0.13 in equation (5.1) of Aghsaee et al. (2010) should be 0.35 and 0.18). We thus applied the criteria of

Boegman et al. (2005) and Aghsaee et al. (2010) to our numerical results to clarify the difference between our study's definition and GBL (Fig. 7). Since a plunging type breaks dynamically at the farthest point offshore and the zero-gravity location is close to the vertical rear of the internal wave, breaking points obtained from numerical simulations are close to the GBL by Aghsaee et al. (2010) in the thin pycnocline cases #-1 (# is P and AP; a_I = 0.01 m). Significantly, surging and collapsing breakers also agree with GBL by Aghsaee et al. (2010) under thin pycnocline conditions (cases #-1, # is S, C, AS and AC). The thin pycnocline case of fission breaker slightly deviates from GBL by Aghsaee et al. (2010) (case F-1). The breaking points for all breaker types slightly differ from GBL by Aghsaee et al. (2010) when pycnocline thickness varies. However, GBL by Aghsaee et al. (2010) appears to fit our numerical simulations satisfactory under changing pycnocline thickness, compared to GBL by Boegman et al. (2005). Therefore, GBL by Aghsaee et al. (2010) could be used to predict the breaking points of an ISW propagating under different pycnocline thickness (S6 in Table 3).

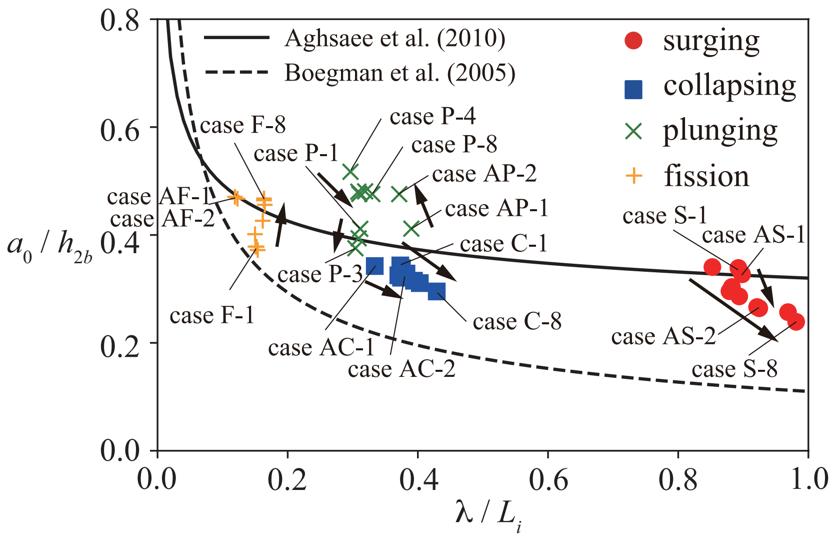

Fig. 7. Breaking points from numerical simulations and breaking criteria by Aghsaee et al. (2010) and Boegman et al. (2005).

3.2. Energy reflection

To observe the effect of pycnocline thickness on breaking from an energetic point of view, we compared energy dissipation by breaking. First, we confirmed that E_K was equal to E_P for incident ISWs for all cases, which supports the validity of the numerical simulations (Fig. 8). We defined the peak ratio of E_T for a reflected internal wave and an incident ISW as “practical reflection coefficient”, C_p. In contrast to the practical reflection coefficient, the “reflection coefficient”, C_{ref}, as defined by Michallet and Ivey (1999) is obtained by integrating the spatial distribution of available potential and kinetic energies (Bourgault and Kelley, 2007). Therefore, when the practical reflection coefficient is much smaller than the reflection coefficient, we can expect that the reflected internal waves consist of a broad range of internal wave frequencies, i.e., we can evaluate the broadening of reflected internal waves from a slope by comparing practical reflection coefficients with reflection coefficients. Therefore, the combination of both reflection coefficients can provide important information about how an ISW deforms into a broad range of internal waves. For the cases with the thinnest pycnocline (a_I = 0.01 m), the practical reflection coefficient was 68 %, 29 %, 11 % and 5 % for surging, collapsing, plunging and fission breakers, respectively, in cases #-1 (# is S, C, P and F; a_I = 0.01 m). In the breaking zone, the peak in E_K was larger than that of the incident ISW for collapsing, plunging and fission breakers (Fig. 8). We conjecture that available potential energy was effectively transferred to kinetic energy due to breaking to a greater extent in collapsing, plunging and fission breakers compared to surging breakers, which resulted in considerably higher energy reflection with surging breakers in the cases of a_I = 0.01 m.

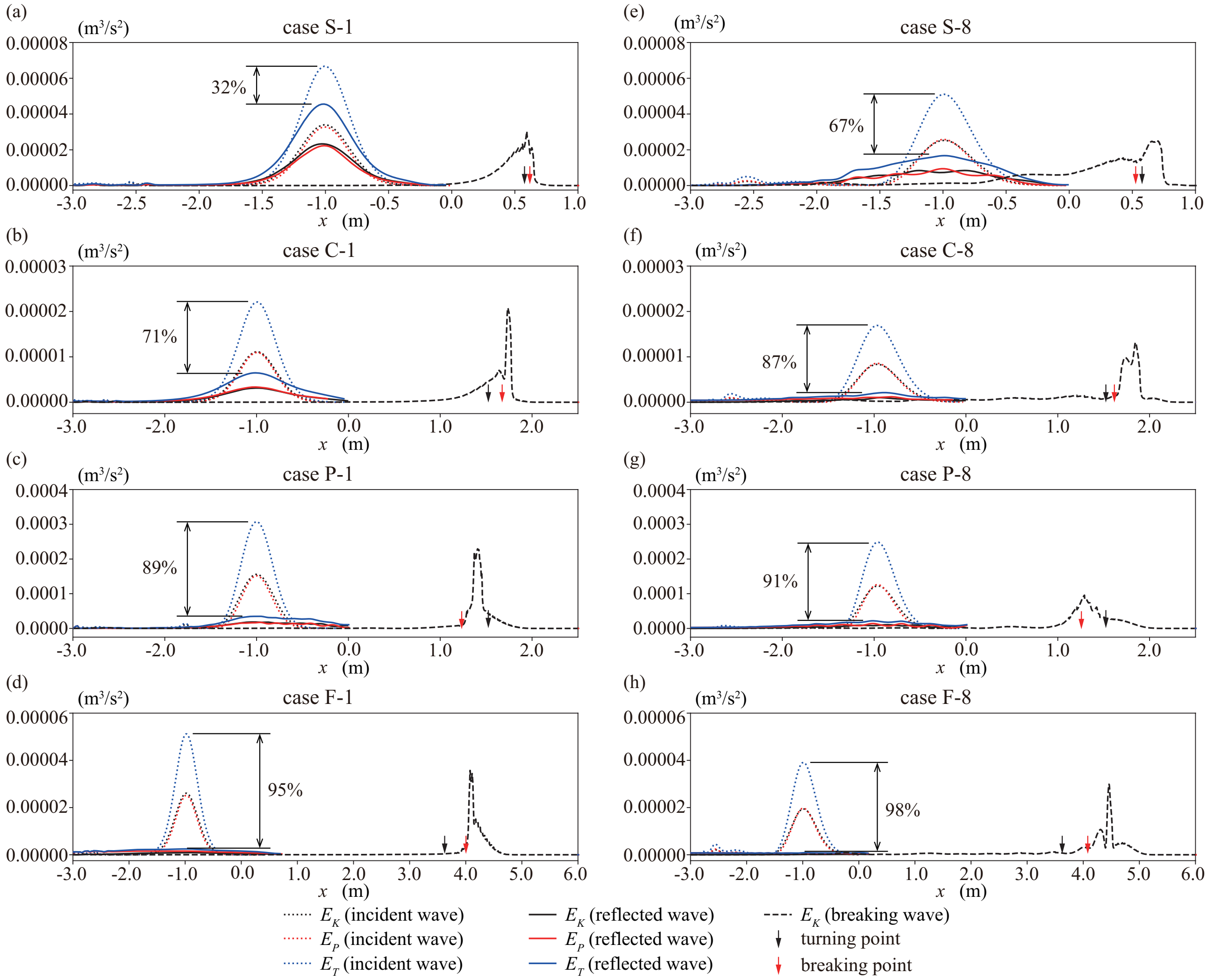

Fig. 8. Potential and kinetic energy of an incident ISW (dots) and a reflected internal wave (solid lines). Kinetic energy in the breaking region (broken lines). (a) Case S-1: Surging breaker. (b) Case C-1: Collapsing breaker. (c) Case P-1: Plunging breaker. (d) Case F-1: Fission breaker. (e) Case S-8: Surging breaker. (f) Case C-8: Collapsing breaker. (g) Case P-8: Plunging breaker. (h) Case F-8: Fission breaker.

In general, an ISW tends to become unstable when the Brunt–Väisälä frequency decreases, which corresponds to thicker pycnocline conditions in this study. Therefore, practical reflection coefficients decreased for all thickness ratios when pycnocline thickness increased (Fig. 8). The practical reflection coefficient was 33 %, 13 %, 9 % and 2 % for surging, collapsing, plunging and fission breakers, respectively, in cases #-8 (# is S, C, P and F; a_I = 0.12 m). Practical reflection coefficients decreased greatly for surging and collapsing breakers in cases #-8 (# is S and C; a_I = 0.12 m) compared to cases #-1 (# is S and C; a_I = 0.01 m) (Fig. 8). In particular, spatially integrated E_K was relatively greater over the slope in the case when a_I = 0.12 m compared to a_I = 0.01 m for surging breakers, in which the practical reflection coefficient decreased most significantly (Fig. 8). Breaking points shifted offshore for surging breaker to a greater extent than for the other breakers, suggesting that more substantial breaking occurred in the surging breaker than the others when pycnocline thickness increased (Fig. 8). Consequently, we conjecture that under thick pycnocline conditions, available potential energy was transferred to kinetic energy over the slope more efficiently for the surging breaker. Therefore, for surging and collapsing breakers, energy decreased more actively due to turbulent dissipation with thicker pycnoclines.

4. DISCUSSION

We found that all classification factors for cases S-#, C-#, P-# and F-# (# = 1 to 8) were valid even with the largest increase in pycnocline thickness. To confirm the applicability of the categorization in Fig. 2, we filled the gap in the classification diagram by adding eight more numerical simulations of extreme pycnocline-thickness cases: AS-#, AC-#, AP-# and AF-# (# = 1 and 2, $a_I = 0.01$ m and $a_I = 0.12$ m) (Table 1 and Table 2). Cases AS-#, AC-#, AP-# and AF-# (# = 1 to 2) are also well categorized into surging, collapsing, plunging and fission breakers according to the classification by Nakayama et al. (2019) (Fig. 2). However, there existed a combination of breakers with increased pycnocline thickness (Figs. 3, 5 and 6). Anti-clockwise and clockwise circulations occurred for a collapsing and plunging breakers clearly when the pycnocline thickness is thin (Figs. 9a and d). The circulations became weaker when the pycnocline thickness increased. In particular, a plunging breaker showed the collapsing characteristic slightly, which is so-called a collapsing-plunging breaker (Fig. 9f). Nevertheless, the clockwise circulation was formed even when pycnocline is the thickest. Therefore, all classification factors were confirmed to be valid even with the largest increase in the pycnocline thickness, and there may be no significant difference in the characteristics of breaker type even when pycnocline thickness varies as summarized in S1, Table 3. Nakayama et al. (2019) demonstrated the classification's applicability into a real stratified fluid using the results of Vlasenko and Hutter (2002). They simulated a plunging breaker under the real scale condition, in which the upper and lower layer thicknesses are 50 m and 950 m. Their result was categorized into a plunging breaker, suggesting the high applicability of Nakayama's classification. Nakayama et al. (2019) also showed that a fission beaker occurs predominantly in a real scale because the natural bottom slope is mild enough to allow fission or plunging breakers due to the high internal Reynolds number. Besides, the applicability of Nakayama's classification to the wide range of real scale conditions remains to be investigated in the future.

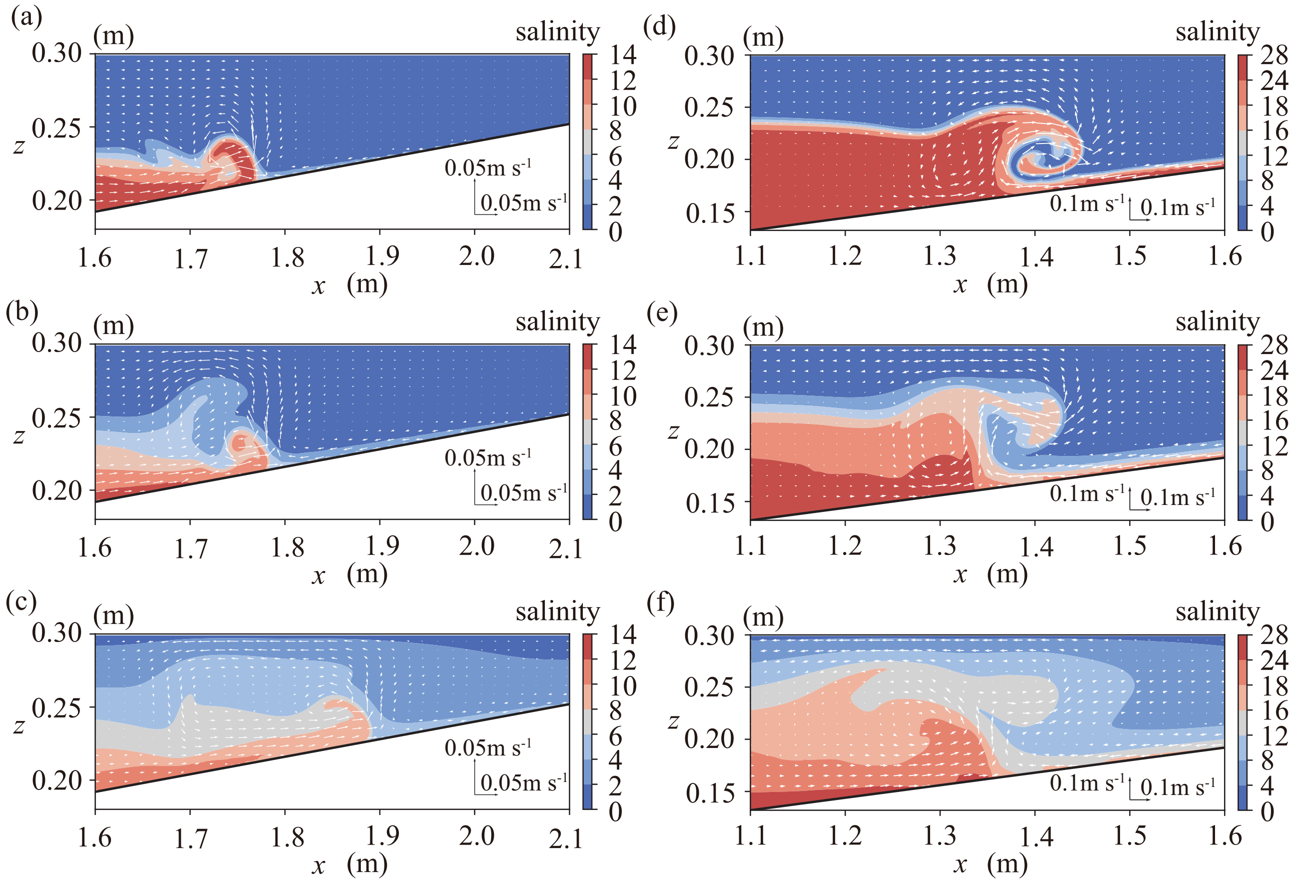

Fig. 9. Velocity vectors. (a) Case C-1: Collapsing breaker. (b) Case P-1: Plunging breaker. (c) Case C-2: Collapsing breaker. (c) Case P-2: Plunging breaker. (e) Case C-6: Collapsing breaker. (f) Case P-6: Plunging breaker.

Table 3. Effect of pycnocline thickness on significant components.
Note that the order of energy dissipation may change since reflection coefficient is a function of the Iribarren number.

		Surging breaker	Collapsing breaker	Plunging breaker	Fission breaker
When pycnocline thickness increases	S1: Breaker type	No change	No change	No change	No change
	S2: Breaking point moves to	Offshore	Offshore	Offshore	Both onshore and offshore
	S3: Practical reflection	Decrease	Decrease	No change	No change

	coefficient				
	S4: Reflection coefficient	Decrease (slightly)	Decrease (slightly)	No change	No change
	S5: Energy transfer from available potential to kinetic energy in a breaking zone	Increase	Increase	No change	No change
S6: Applicability of GBL to estimate breaking point	Thin pycnocline	Good	Good	Good	Satisfactory
	Thick pycnocline	Satisfactory	Satisfactory	Satisfactory	Satisfactory
S7: Applicability of the Iribarren number to model reflection coefficient	Thin pycnocline	Good	Good	Good	Good
	Thick pycnocline	Satisfactory	Satisfactory	Good	Good
S8: Energy dissipation over a slope	Greater, in order	4	3	2	1

As shown in cases S-#, C-#, P-# and F-# (# is 1 to 8), all breaking points for cases AS-#, AC-#, AP-# and AF-# (# = 1 to 2) appeared below the critical depth (Fig. 4). Also, the breaking points of collapsing and fission breakers appeared onshore from the turning point. The surging breaking point occurred close to the turning point, and the plunging breaking point occurred offshore from the turning point. When pycnocline thickness increased, breaking points for all breakers shifted offshore in cases AS-#, AC-#, AP-# and AF-# (# = 1 to 2) (Fig. 4). In the fission breakers (cases F-#, # = 1 to 8), the breaking points shifted onshore when pycnocline thickness increased. Therefore, excluding fission breakers, breaking points are likely to shift offshore with an increase in the pycnocline thickness (S2 in Table 3).

For the reflection of the internal waves from the sloping boundary, Nakayama and Imberger (2010) demonstrated that the reflection coefficient of internal waves tends to become zero in a two-layer fluid of equivalent depth when the amplitude of an incident internal wave is more than the critical amplitude. The practical reflection coefficient was 29 % in case C-1, which represents conditions similar to the case by Nakayama and

Imberger (2010) when the reflection coefficient was zero. This is because Nakayama and Imberger (2010) used sinusoidal internal waves propagated over a flat bottom using the same water depth setup in a two-layer fluid. An ISW may reflect more than a sinusoidal-type internal wave.

Energy dissipation due to the breaking of an ISW over a slope is one of the most significant issues in the ocean (Michallet and Ivey, 1999; Bourgault et al., 2007). Therefore, we computed the time series of the spatially-integrated available potential and kinetic energies, Φ_P and Φ_K, by integrating available potential and kinetic energies, E_P and E_K, horizontally from offshore to the breaking point (in a non-breaking zone). Regarding E_K, we also obtained the spatially-integrated kinetic energy, Ψ_K, by integrating kinetic energy, E_K, in the region from the breaking point to the most onshore point (in a breaking zone) (Fig. 9). Here, $\Phi_T = \Phi_P + \Phi_K$ and we define "reflection coefficient", C_{ref}, which is the ratio of Φ_T for a reflected internal wave and an incident ISW. Our definition of reflection coefficient corresponds to that of the reflection coefficient by Michallet and Ivey (1999) and Bourgault et al. (2007). Reflection coefficients were greater, in order, for surging, collapsing, plunging and fission breakers under thin pycnocline conditions (Fig. 9). A surging breaker with a_I = 0.01 m had the maximum reflection coefficients of 86 % in case S-1 and 82 % in case AS-1. When a_I = 0.01 m, the minimum reflection coefficients were 25 % (case F-1) and 17 % (case AF-1) in a fission breaker, which was higher than the practical reflection coefficients, 5 % and 3 %, because the wavelength of the reflected internal wave had broader range frequencies than the incident ISW, which results in the reduction of the peak of total energy in the reflected internal wave. When a_I = 0.12 m, surging and collapsing breakers had larger decreases in reflection coefficients compared to the other breakers with a_I = 0.01 m. Concerning the spatially-integrated kinetic energy, Ψ_K, in the breaking zone, the thicker the pycnocline, the larger the Ψ_K for surging and collapsing breakers. We conjecture that available potential energy over a slope was transferred to kinetic energy by breaking, which enhances energy dissipation and decreases reflection coefficients when pycnocline thickness increased for surging and collapsing breakers.

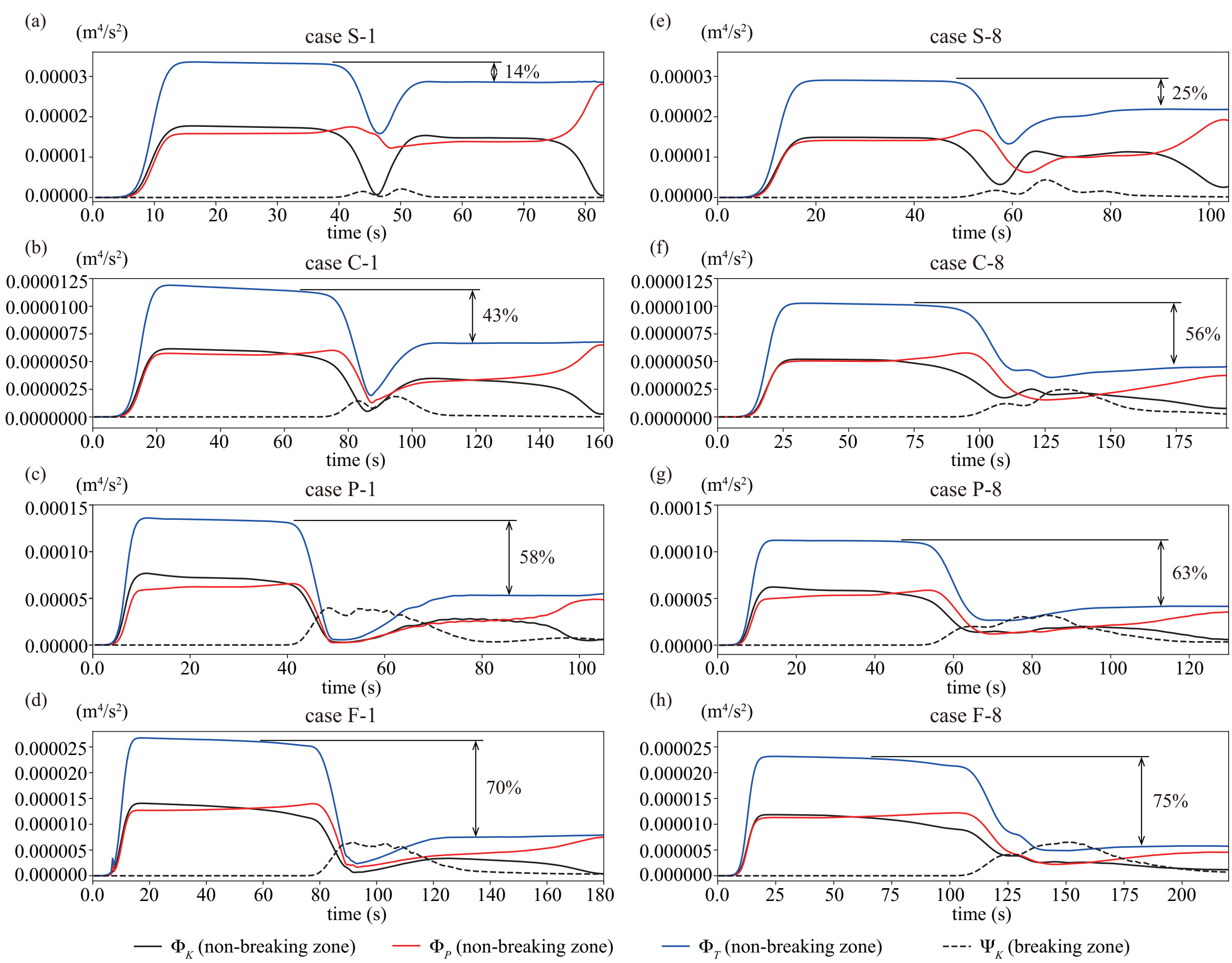

Fig. 10. Φ_K, Φ_P and Φ_T in a non-breaking zone, and Ψ_K in a breaking zone. (a) Case S-1: Surging breaker. (b) Case C-1: Collapsing breaker. (c) Case P-1: Plunging breaker. (d) Case F-1: Fission breaker. (e) Case S-8: Surging breaker. (f) Case C-8: Collapsing breaker. (g) Case P-8: Plunging breaker. (h) Case F-8: Fission breaker.

Practical reflection coefficients provide essential information on the internal wave reflected from a slope for the investigation of real scale phenomena. Therefore, we attempted to clarify the effect of pycnocline thickness on practical reflection coefficients (Fig. 10). Practical reflection coefficients dramatically decreased until the pycnocline thickness equaled to the upper layer thickness $\alpha_I/h_1 < 1.0$ for surging and collapsing breakers, and became almost constant in the range of $\alpha_I/h_1 \geq 1.0$ (Fig. 10a) (S3 in Table 3). In contrast, the practical reflection coefficients were less than 10 % and did not change under varying pycnocline thickness for plunging and fission breakers (S3 in Table 3). On the other hand, spatially-integrated energy dissipation, i.e., the reflection coefficient, is also vital for real scale modelling. Reflection coefficients were higher, in order, for surging, collapsing, plunging and fission breakers in the same manner as practical reflection coefficients in this study (S8 in Table 3). Interestingly, the reflection coefficients were almost constant under changing pycnocline thickness for plunging and fission breakers, but changed slightly in the range from $\alpha_I/h_1 = 0$ to $\alpha_I/h_1 = 0.6$ for surging and collapsing breakers because of the offshore shift in breaking points, which makes breaking more dynamic (Fig. 10b) (S4 in Table 3). Interestingly, the difference between C_p and C_{ref} for surging and collapsing breakers became more remarkable with an increase in the pycnocline thickness. Thus, we conjecture that energy is transferred to a broad range of frequencies due to the ISW breaking for surging and collapsing breakers to a greater extent than plunging and fission breakers under thick pycnocline conditions compared to thin pycnocline condition (S5 in Table 3).

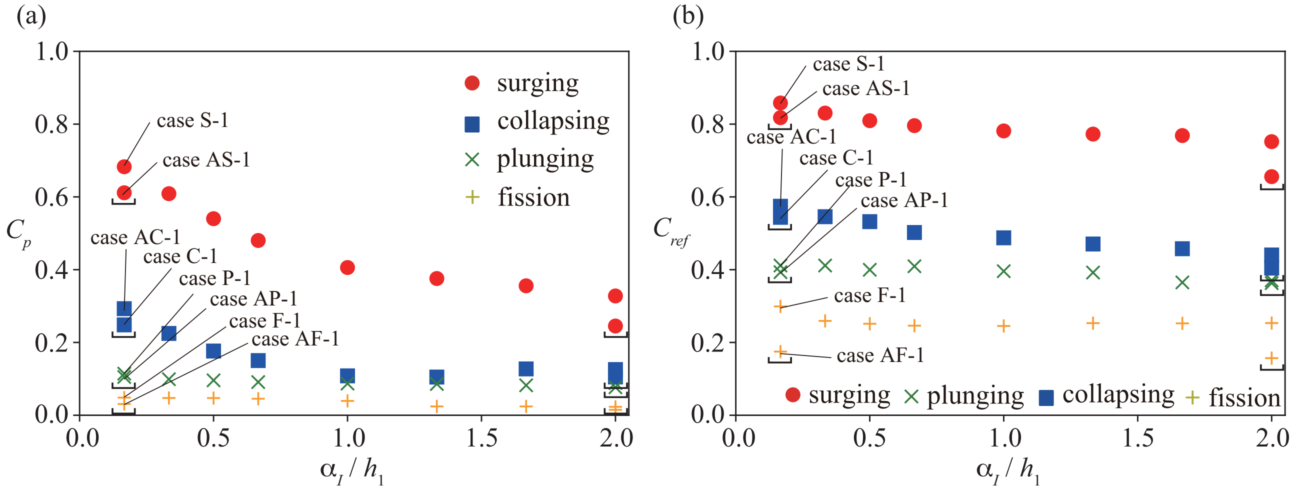

Fig. 11. (a) Practical reflection coefficient, C_p, and pycnocline thickness. (b) Reflection coefficient, C_{ref}, and pycnocline thickness. Pycnocline thickness is normalized by the upper layer depth. Under bars correspond to cases #-1 and #-2 (# = 5 to 8).

Michallet and Ivey (1999) demonstrated that the reflection coefficient was a function of λ/L. Note that their experimental conditions were categorized as plunging breakers using the classification indices by Nakayama et al. (2019). The reflection coefficients presented in this study are slightly larger, but those for plunging cases are close to their laboratory experiment results (Fig. 11a). Chen et al. showed the similar tendency as our results, in which the reflection coefficients obtained from the laboratory experiments were slightly larger than Michallet and Ivey. On the other hand, Bourgault and Kelly (2007) investigated the reflection coefficient using the same conditions as Michallet and Ivey (1999), showing that the reflection coefficient is a function of the internal Iribarren number

($\xi_I = S/\sqrt{S_w}$). Our results appeared to agree with the criteria of Bourgault and Kelly (2007) better than Michallet and Ivey (1999), which suggests the high applicability of the following equation to thin pycnocline conditions (Fig. 11b) (S7 in Table 3).

$$C_{ref} = 1 - \exp(-\xi_I). \tag{8}$$

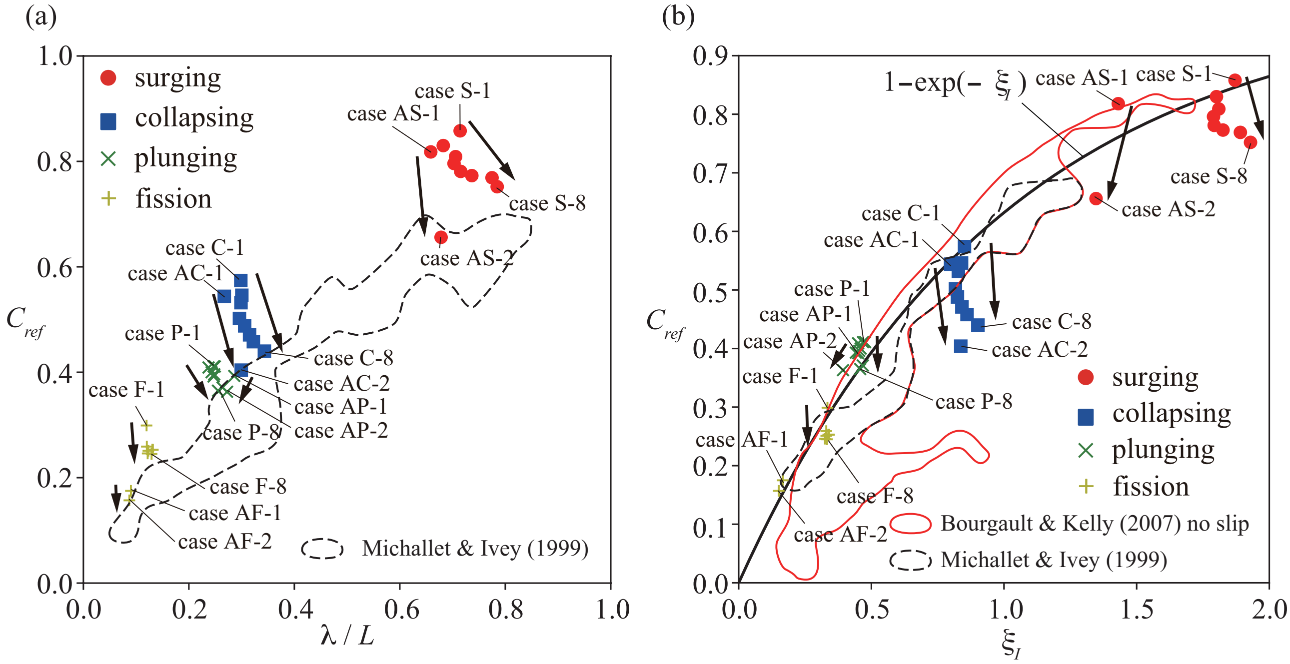

Fig. 12. Comparisons of reflection coefficient. (a) λ/L and C_{ref} by Michallet et al. (1999). (b) ξ_I and C_{ref} by Bourgault et al. (2007).

In thick pycnocline conditions, reflection coefficients are slightly smaller for surging and collapsing breakers compared to Eq. (10). However, all cases agree well with Eq. (10). Since Aghsaee et al. (2010), Sutherland et al. (2013) and Nakayama et al. (2019) suggested that the internal Iribarren number has difficulty in capturing the characteristics of breaker types for an ISW over a slope, further research is needed to confirm the validity of the relationship between the reflection coefficient and the internal Iribarren number.

5. CONCLUSIONS

This study investigated the effect of breaker type on energy dissipation due to an ISW breaking over a uniform slope when pycnocline thickness varies (Table 3). We showed the possibility of classifying ISW breaking into surging, collapsing, plunging and fission breakers using bottom slope gradient, wave slope and the internal Reynolds number proposed by Nakayama et al. (2019) even when the pycnocline thickness reaches the water surface. Practical reflection coefficients became smaller with the increase in pycnocline thickness for surging and collapsing breakers, while it was constant for plunging and fission breakers under changing pycnocline thickness. On the other hand, the reflection coefficient of spatially-integrated energy from a slope did not change significantly under varying pycnocline thickness, except for a slight decrease for surging and collapsing breakers when pycnocline thickness increased. The definition of GBL by Aghsaee et al. (2010) could be used to predict the breaking points of an ISW propagating under different pycnocline thickness. The reflection coefficient of an ISW from a slope may be estimated as a function of the Iribarren number even for thick pycnocline cases. Note that our two-dimensional simulations may underestimate 8 % energy dissipation than a three-dimensional simulation, as demonstrated in Arthur and Fringer (2014).

Acknowledgements

This work was supported by the Japan Society for the Promotion of Science under grant 18H01545 and 18KK0119.

Data Availability Statement

The data that support the findings of this study are available from the corresponding author upon reasonable request.

REFERENCES

Adcroft, A.J., Hill, C., Marshall, J., 1997. Representation of topography by shaved cells in a height coordinate ocean model. Mon. Wea. Rev. 125, 2293-2315.

Aghsaee, P., Boegman, L., Diamessis, P.J., Lamb, K.G., 2012. Boundary-layer-separation-driven vortex shedding beneath internal solitary waves of depression. J. Fluid Mech. 690, 321-344.

Aghsaee, P., Boegman, L., Lamb, K.G., 2010. Breaking of shoaling internal solitary waves. J. Fluid Mech. 659, 289-317.

Arthur, R.S., Fringer, O.B., 2014. The dynamics of breaking internal solitary waves on slopes. J. Fluid Mech. 761, 360-398.

Boegman, L., Ivey, G.N., Imberger, J., 2005. The degeneration of internal waves in lakes with sloping topography. Limnol. Oceanogr. 50, 1620-1637.

Boegman, L., Stastna, M., 2019. Sediment resuspension and transport by internal solitary waves. Annu. Rev. Fluid Mech. 51, 129-154.

Bourgault, D., Kelley, D.E., 2007. On the reflectance of uniform slopes for normally incident interfacial solitary waves. J. Phys. Oceanogr. 37, 1156-1162.

Chen, C.Y., Hsu, J.R.C., Cheng, M.H., Chen, H.H., Kuo, C.F., 2007. An investigation of internal solitary waves in a two-layer fluid: Propagation and reflection from steep slopes. Ocean Eng. 34, 171-184.

Davis, K.A., Monismith, S.G., 2011. The modification of bottom boundary layer turbulence and mixing by internal waves shoaling on a barrier reef. J. Phys. Oceanogr. 41, 2223-2241.

Dean, R.G., Dalrymple, R.A., 1991. Water wave mechanics for engineers and scientists. In Advanced Series on Ocean Engineering (d. L. F. Liu). vol 2, World Scientific, America.

Forgia, G., Tokyay, T., Adduce, C., Constantinescu, G., 2018. Numerical investigation of breaking internal solitary waves. Phys. Rev. Fluids. 3, 104801.

Forgia, G., Ottolenghi, L., Adduce, C., Falcini, F., 2020. Intrusions and solitons: Propagation and collision dynamics. Phys. Fluids 32, 076605.

Galvin, C.J., 1968. Breaker type classification on three laboratory beaches. J. Geophys. Res. 73, 3651-3659.

Gloor, M., Wuest, A., Munnich, M., 1994. Benthic boundary mixing and resuspension induced by internal seiches. Hydrobiologia 284, 59-68.

Helfrich, K.R., 1992. Internal solitary wave breaking and run-up on a uniform slope. J. Fluid Mech. 243, 133-154.

Helfrich, K.R., Melville, W.K., 2006. Long nonlinear internal waves. Annu. Rev. Fluid Mech. 38, 395-425.

Horn, D.A., Imberger, J., Ivey, G.N., 2001. The degeneration of large-scale interfacial gravity waves in lakes. J. Fluid Mech. 434, 181-207.

Jones, W.P., Launder, B.E., 1972. The prediction of laminarization with a two-equation model of turbulence. Int. J. Heat Mass Transfer 15, 301-314.

Koop, C.G., Butler, G., 1981. An investigation of internal solitary waves in a two-fluid system. J. Fluid Mech. 112, 225-251.

Lamb, K.G., 2014. Internal wave breaking and dissipation mechanisms on the continental slope/shelf. Annu. Rev. Fluid Mech. 46, 231-254.

Lamb, K.G., Wan, B., 1998. Conjugate flows and flat solitary waves for a continuously stratified fluid. Phys. Fluids 10, 2061-2079.

Michallet, H., Ivey, G.N., 1999. Experiments on mixing due to internal solitary waves breaking on uniform slopes. J. Geophys. Res. 104, 13467-13477.

Mirie, R.M., Pennell, S.A., 1989. Internal solitary waves in a two-fluid system. Phys. Fluids A1, 986-991.

Nakayama, K., Imberger, J., 2010. Residual circulation due to internal waves shoaling on a slope. Limnol. Oceanogr. 55, 1009-1023.

Nakayama, K., Kakinuma, T., Tsuji, H., 2019. Oblique reflection of large internal solitary waves in a two-layer fluid. Euro. J. Mech. B/Fluids 74, 81-91.

Nakayama, K., Lamb, K.G., 2020. Breathers in a three-layer fluid. J. Fluid Mech. 903 (A40).

Nakayama, K., Nguyen, H.D., Shintani, T., Komai, K., 2016. Reversal of secondary circulations in a sharp channel bend. Coast. Eng. J. 58, 1650002.

Nakayama, K., Sato, T., Shimizu, K., Boegman, L., 2019. Classification of internal solitary wave breaking over a slope. Phys. Rev. Fluids. 4, 014801.

Nakayama, K., Shintani, T., Kokubo, K., Kakinuma, T., Maruya, Y., Komai, K., Okada, T., 2012. Residual current over a uniform slope due to breaking of internal waves in a two-layer system. J. Geophys. Res. 117 (C10002).

Nakayama, K., Shintani, T., Shimizu, K., Okada, T., Hinata, H., Komai, K., 2014. Horizontal and residual circulations driven by wind stress curl in Tokyo Bay. J. Geophys. Res. 119, 1977-1992.

Pierson, D.C., Weyhenmeyer, G.A., 1994. High resolution measurements of sediment resuspension above an accumulation bottom in a stratified lake. Hydrobiologia 284, 43-57.

Pineda, J., 1994. Internal tidal bores in the nearshore: Warm-water fronts, seaward gravity currents and the onshore transport of neustonic larvae. J. Mar. Res. 52, 427-458.

Saffarinia, K., Kao, T.W., 1996. Numerical study of the breaking of an internal soliton and its interaction with a slope. Dyn. Atmos. Oceans 23, 379-391.

Shroyer, E.L., Moum, J.N., Nash, J.D., 2009. Observations of polarity reversal in shoaling nonlinear internal waves. J. Phys. Oceanogr. 39, 691-701.

Sutherland, B.R., Barrett, K.J., Ivey, G.N., 2013. Shoaling internal solitary waves. J. Geophys. Res. 118, 4111-4124.

Taileux, T., 2013. Available Potential Energy and Exergy in Stratified Fluids. Annu. Rev. Fluid Mech. 45, 35-58.

Tsuji, H., Oikawa, M., 2007. Oblique interaction of solitons in an extended Kadomtsev-Petviashvili equation. J. Phys. Soc. Jpn. 76, 84401-84408.

Umlauf, L., Burchard, H., 2003. A generic length-scale equation for geophysical turbulence models. J. Mar. Res. 61, 235-265.

Vlasenko, V., Hutter, K., 2002. Numerical experiments on the breaking of solitary internal waves over a slope-shelf topography. J. Phys. Oceanogr. 32, 1779-1793.